Available online at www.sciencedirect.com
SCIENCE DIRECT®
International Journal of Solids and Structures 42 (2005) 565–579
INTERNATIONAL JOURNAL OF SOLIDS and STRUCTURES
www.elsevier.com/locate/ijsolstr

Numerical experiments on the rupture of brittle solids—variation of microstructure, loading and dimensions

Ioannis Doltsinis *, Rainer Dattke

Faculty of Aerospace Engineering, University of Stuttgart, Pfaffenwaldring 27, D70569 Stuttgart, Germany

Received 29 April 2004; received in revised form 14 June 2004
Available online 27 August 2004

Abstract

The significance of microstructural parameters for the damage and rupture of brittle materials is investigated by a numerical model that accounts for separation of grain interfaces. The microcracking approach refers to a specified material structure; synthetic random sampling allows for fluctuations. Thus, damage progression is simulated and the strength of material specimens is estimated by employing fracture mechanics within a microstructure that exhibits statistical variability. The issues addressed regard failure behaviour, strength level and sensitivity to microstructural parameters. Also discussed is the effect of specimen dimensions in connection with rupture.

Keywords: Brittle materials; Micromechanics; Numerical modelling; Damage; Rupture

1. Introduction

The study deals with the rupture of brittle materials as resulting from fracturing processes on the microscopic level. The absence of a mature continuum theory on the progressive damage and rupture of otherwise elastic solids suggests considerations on the microscopic level accounting for the material structure to the extent that circumstances require. The necessity to model on the microscale for investigating macroscopic behaviour appears moreover helpful in fundamentally exploring links between the two different levels of observation: whenever we feel not to be in the position to establish rules from observations at a certain level or are interested in background reasoning, we recall that we may register the collective result

* Corresponding author. Tel.: +49 7116857788; fax: +49 7116853644.
E-mail address: doltsinis@ica.uni-stuttgart.de (I. Doltsinis).

0020-7683/$ - see front matter
doi:10.1016/j.ijsolstr.2004.06.049

of events or processes taking place at a lower level and measured at a finer scale. Micromechanical approaches particularly relevant to the present work comprise the treatment of interacting cracks developed by Kachanov (1987), the accounting for other cavities (Kachanov et al., 1994) and the study of pore interaction (Tsukrov and Kachanov, 1997). A most interesting result of the latter investigation concerns the locations in the material prone to fracturing. Beyond this discussion on incipient fracture, the numerical algorithm described by Doltsinis (1998) models progressive fracturing in the microstructure. The methodology has been extended later to the rupture of porous materials subject to internal pressure (Doltsinis and Dattke, 2001).

The present account starts with a constitutive framework for the fracturing continuum and indicates the interface with micromechanics (Doltsinis, 1998). Numerical investigations (Doltsinis, 1998; Dattke, 2003) show that, depending on the material structure, an initially distributed mode of fracturing begins to localize sooner or later in the course of the loading. The microcrack pattern that then forms determines the ultimate failure of the material specimen. Rupture modes resulting from micromechanical computations for various types of loading are seen to agree with intuition and reasoning. The synergy towards rupture provided by crack interaction is demonstrated as is also the degree of brittleness in dependence of the topological details at given overall parameters. When moving from conditions that favour gradually developing, quasi-brittle failure to such favouring rather sudden, brittle rupture, the scatter of observations related to strength becomes a significant companion of the spatial variability of the microstructure and is considered an intrinsic feature of the material. In this context the probability of a particular event to occur is of interest rather than mean values and scatter of properties.

Exploration of randomness in the present context is performed by means of synthetic sampling of the microstructure. An exemplary investigation that concerns porous material subject to internal fluid pressure, refers to the random topology of the pores. Apart from the effect of size and shape of pores the influence of the specimen dimensions has been of interest with regard to the representative volume element of the material. The results of the numerical experiments are discussed on the background of Weibull statistics (Weibull, 1951).

2. Fracturing continuum

Let the effect of homogeneously distributed microcracks on the response of an elastic material be characterized by a number of parameters collected in the column matrix (vector) $\mathbf{D}$. The relations

$$\boldsymbol{\sigma}(\boldsymbol{\varepsilon}, \mathbf{D}) = \boldsymbol{\kappa}(\mathbf{D})\boldsymbol{\varepsilon} \tag{1}$$

and

$$\dot{\boldsymbol{\sigma}} = \boldsymbol{\kappa}(\mathbf{D})\dot{\boldsymbol{\varepsilon}} + \dot{\boldsymbol{\kappa}}(\mathbf{D})\boldsymbol{\varepsilon}, \tag{2}$$

between the 6×1 vector arrangements of stress $\boldsymbol{\sigma}$ and of strain $\boldsymbol{\varepsilon}$ describe linear elastic behaviour as long as $\mathbf{D} = \text{constant}$. Otherwise the elasticity matrix $\boldsymbol{\kappa}(\mathbf{D})$ of the material is affected in the course of the loading process and reflects on the time rate. The energy difference between loading and elastic unloading of the unit material volume element is

$$\mathscr{G} = \int_0^{\varepsilon} \boldsymbol{\sigma}^{\mathrm{t}} \mathrm{d}\boldsymbol{\varepsilon} - \frac{1}{2}\boldsymbol{\sigma}^{\mathrm{t}}\boldsymbol{\varepsilon}. \tag{3}$$

The difference vanishes if fracturing does not occur. The rate quantity

$$\dot{\mathscr{G}} = -\frac{1}{2}\boldsymbol{\varepsilon}^{\mathrm{t}}\dot{\boldsymbol{\kappa}}(\mathbf{D})\boldsymbol{\varepsilon}, \tag{4}$$

gives the temporal rate of energy release due to the progression of fracture in the unit volume element of the material. If an area A is assigned collectively to the system of distributed microcracks, the energy consumption per unit fractured area is 2γ, where γ denotes the specific surface energy of the material. Comparison of energy release and consumption for a virtual increment δA suggests that fracturing will not progress as long as

$$\Delta\mathscr{G} = \frac{\mathrm{d}\mathscr{G}}{\mathrm{d}A}\delta A + \frac{1}{2}\frac{\mathrm{d}^2\mathscr{G}}{\mathrm{d}A^2}\delta A^2 \leqslant 2\gamma\delta A. \tag{5}$$

Detailing first and second order terms, a fracturing criterion can be introduced based on the energy release rate

$$G = \frac{\mathrm{d}\mathscr{G}}{\mathrm{d}A} = -\frac{1}{2}\boldsymbol{\varepsilon}^{\mathrm{t}}\frac{\mathrm{d}\boldsymbol{\kappa}(\mathbf{D})}{\mathrm{d}A}\boldsymbol{\varepsilon} = \frac{1}{2}\boldsymbol{\sigma}^{\mathrm{t}}\frac{\mathrm{d}\boldsymbol{\kappa}^{-1}(\mathbf{D})}{\mathrm{d}A}\boldsymbol{\sigma}. \tag{6}$$

In stress space, for instance, the fracturing resp. non-fracturing condition is stated as

$$\Phi(\boldsymbol{\sigma},\mathbf{D}) = G(\boldsymbol{\sigma},\mathbf{D}) - 2\gamma \leqslant 0. \tag{7}$$

The fracture surface $\Phi(\boldsymbol{\sigma},\mathbf{D}) = 0$ limits the domain of elastic stress states. During fracturing the consistency condition observed on the surface

$$\frac{\mathrm{d}\Phi}{\mathrm{d}A} = \frac{\mathrm{d}G}{\mathrm{d}A} = \frac{\mathrm{d}^2\mathscr{G}}{\mathrm{d}A^2} = 0, \tag{8}$$

controls the second order term of Eq. (5).

Actually, the microcrack system affects the elasticity matrix of the material via the parameters in $\mathbf{D}$. Analytical developments (Kachanov, 1987) base on the contribution $\boldsymbol{\varepsilon}_{\mathrm{c}}$ of cracks to the overall strain:

$$\boldsymbol{\varepsilon} = \boldsymbol{\kappa}_0^{-1}\boldsymbol{\sigma} + \boldsymbol{\varepsilon}_{\mathrm{c}} = [\boldsymbol{\kappa}_0^{-1} + \mathbf{M}(\mathbf{D})]\boldsymbol{\sigma} = \boldsymbol{\kappa}^{-1}(\mathbf{D})\boldsymbol{\sigma}. \tag{9}$$

In the above, the elasticity matrix $\boldsymbol{\kappa}_0$ refers to the material without cracks, while the matrix operator $\mathbf{M}(\mathbf{D})$ furnishes at state $\mathbf{D}$ the excess strain $\boldsymbol{\varepsilon}_{\mathrm{c}}$ for an imposed stress $\boldsymbol{\sigma}$. The energy release rate of Eq. (6) thus becomes

$$G = \frac{1}{2}\boldsymbol{\sigma}^{\mathrm{t}}\frac{\mathrm{d}\boldsymbol{\kappa}^{-1}(\mathbf{D})}{\mathrm{d}A}\boldsymbol{\sigma} = \frac{1}{2}\boldsymbol{\sigma}^{\mathrm{t}}\frac{\mathrm{d}\mathbf{M}(\mathbf{D})}{\mathrm{d}A}\boldsymbol{\sigma}, \tag{10}$$

and can be evaluated along the direction of change of $\mathbf{D}$ for which fracturing is momentarily explored. This presumes definition of the actual state $\mathbf{D}$, availability of the functional dependence $\mathbf{M}(\mathbf{D})$, and determination of $\mathrm{d}\mathbf{D}/\mathrm{d}A$ along the trial direction of fracture progress. Any release of stored energy of eigenstrains adds to G or equally diminishes 2γ (Doltsinis, 1998).

3. Computer simulation on the microscale

Utilization of the constitutive framework for the fracturing continuum presented in Section 2 relies on the impact of the microcrack system on the elastic compliance of the material, resp. on its stiffness. This has been detailed by Kachanov (1987) and has been exemplified for the overall properties in the presence of certain arrangements. But, rather arbitrary crack patterns and examination of the stability of the system with respect to further fracturing may demand discrete numerical models capable of computational treatment. This issue has been dealt with in extenso by Doltsinis (1998), and the employment of computer modelling for completing the constitutive framework was shown. In this connection, the stability analysis can be

performed by directly computing energy changes instead of employing the elastic compliance in dependence of the progressing fracture as in Eq. (10).

The path-dependent non-linear effects of crack closure and frictional sliding complicate the situation, thus necessitating numerical modelling and computer simulation of processes taking place in the microstructure. Moreover, the applicability of a material constitutive approach that presumes distributed cracks is limited by the formation of distinct crack patterns, and so is also its utility in describing failure by degradation of local mechanical properties.

Several numerical models of brittle material behaviour are surveyed in the literature (Krajcinovic, 1996). The two approaches described in the following differ by the way that structural characteristics of the material enter the computation system. The one projects such properties onto a network of elastic bars, the other works immediately on a virtual microstructure. We first mention *en passant* modelling by the elastic bar network before focusing on the direct representation of the material structure.

3.1. Network of elastic bars

The modelling of elastic continua by frameworks of bars discussed by Hrennikoff (1941), requires some caution with respect to the reproduction of overall elastic behaviour, as for instance isotropy, and the appertaining material constants. In particular, Poisson's ratio is difficult to adjust since it is mostly fixed by the pattern of the unit cell employed. The elastic bar (or elastic spring) technique appears interesting for the present purposes because microstructural characteristics can be projected onto a simple computational model. Thus, elastic modulus, initial strains, and ultimate strength can be allocated to the individual bar elements in accordance with given probability distributions.

In connection with the model, it is worth mentioning reports on early work (Louis et al., 1986; Srolovitz and Beale, 1988), and the survey of developments (Krajcinovic, 1996). The following remarks refer to as yet unpublished results obtained within the limitations of a diploma thesis (Treiniés, 1988). Figs. 1 and 2 display in a computational grid damage patterns for a ceramic specimen in two dimensions. Without going into details, the grid consists of equal-sited triangular cells formed of elastic bars, 5 μm long. The triangular cells fix Poisson's ratio of the regular elastic grid to the value of 1/3. The ultimate strength allocated to the individual bars follows a truncated Gaussian probability distribution. Bars break irreversibly once the respective strength is exceeded, and the computation is repeated at constant load level until the crack pattern stabilizes. Otherwise, rupture of the specimen is indicated and the load cannot be augmented anymore.

Fig. 1 shows results for damage under extension along the vertical axis. Broken bar elements have been eliminated in the plot. The initially rather distributed pattern in the left frame is seen to localize and later to form a crack normal to the imposed strain (right frame). Fig. 2 displays stages of damage under imposed

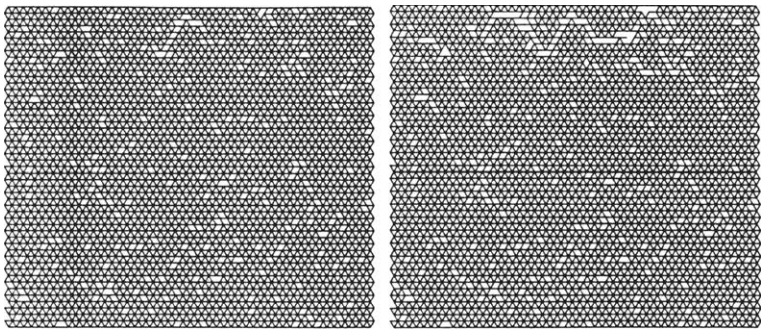

Fig. 1. Damage patterns computed for vertical extension (left: early stage, right: advanced stage).

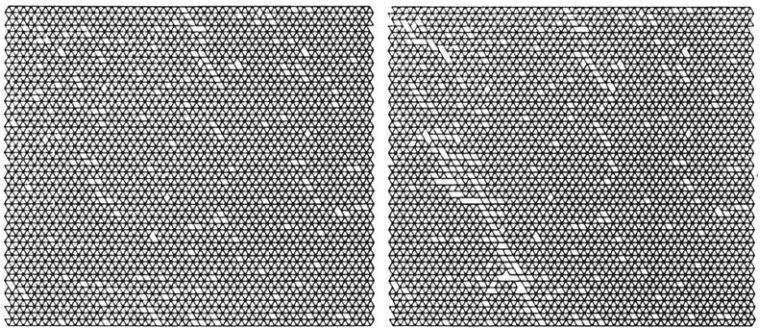

Fig. 2. Damage patterns computed for imposed shear strain $\rightleftharpoons$ (left: early stage, right: advanced stage).

shear. The advanced stage on the right-hand side is characterized by the appearance of a pronounced oblique crack, not predictable from the early distributed pattern shown on the left. Localization of damage is ascribed to the synergetic action of the bar elements in the grid assembly.

Apart from the deficiency of the bar model to reproduce the macroscopic properties of an arbitrary elastic continuum, there are certain difficulties related to the simulation of damage on the microscale. To be specific, elimination of broken elements can lead to local kinematic mechanisms not tolerated in the static solution. Introducing, instead, a considerable diminution of elastic modulus does not necessarily avoid the numerical problems. On the other hand, the triangular unit cell employed in the study does not exhibit isotropic behaviour: for straining along a bar element the stresses are higher than if the strain is applied perpendicular to it. Therefore, the orientation of the grid influences the evolution of damage in the present microstructural approach.

3.2. Modelling of the microstructure

The computational algorithm described in the following (Doltsinis, 1998) considers fracturing in a given material structure. The algorithm operates on a two-dimensional geometrical model of the microstructure generated in the computer, which consists of grains appertaining to the different material phases and pores of various shapes (Doltsinis and Dattke, 2001). Assuming intergranular fracture, the grain interfaces constitute a network of potential cracks that may nucleate under the action of loads. Elementary stress solutions for cavities compiled from the literature supplement the stress disturbances emanating from interacting cracks (Kachanov, 1987) in order to estimate the straining of grain interfaces. At each incremental step during the loading programme the algorithm computes the tractions along grain interfaces while the kinematic activity of cracks is considered with regard to crack closure and frictional sliding.

Separation of grain interfaces is based on the Griffith energy criterion employed here for discrete microcracking in the material: it is assumed that the jth grain interface of length l_j fails completely and forms a crack if

$$\int_j G\mathrm{d}l \geqslant (2\gamma + \epsilon)_j l_j. \tag{11}$$

In the two-dimensional system the elastic energy G is released per unit crack length during virtual separation of the grain interface. Evaluation is simple: it can be based on the average tractions along the interface actually computed at the state of loading under consideration; if the material is stressed by internal pressure in the pores, stress intensity factors are used instead as available for pore/crack combinations (Doltsinis and Dattke, 2001). The specific surface energy γ may vary among grain interfaces. It is reduced by the diminution ϵ of stored energy due to eigenstrains, usually of thermal origin from manufacturing.

Computer simulations underline that the process of brittle microcracking and rupture reflects the antagonism between structural disorder and the steering action of the applied forces. As a rule, tension implies brittle behaviour; failure occurs by specimen separation essentially perpendicular to the applied stress. In the presence of eigenstrains randomly distributed in the grain structure, microcracking first occurs in a distributed manner. Cracks localize and lead to separation at higher tensile stress depending on the intensity of the eigenstrain field (Doltsinis, 1998). When the energy release from the eigenstrains counterbalances the specific surface energy ($\epsilon = -2\gamma$) separation of grain interfaces can occur spontaneously, the applied stress having a catalytic action. Failure under compressive stress is preceded by a phase of distributed fracturing, until microcracks localize to a band across the specimen. Localization is seen to be a consequence of synergy between separating grain interfaces. As demonstrated in Fig. 3 (upper part) for vertical compression of a compact two-phase material, initial cracks appearing in the middle part of the specimen attract subsequent nucleations such that an appreciable oblique band is formed. The nature of compressive loading hinders crack opening. The separation of grain interfaces here gives rise to sliding motion where friction usually delays damage. The displayed material structure represents a single realization out of a statistical sample comprising 500 units that differ as for the topology of the grain phases (fine/coarse) while maintaining overall characteristics. The lower part of Fig. 3 refers to computations where interactions have been suppressed in the model for the purpose of demonstration. This leads to randomly distributed microcracks, the same crack density is now obtained at higher compressive stress. Scatter in the stress value is reduced, such that synthetic sampling stabilizes after 200 random realizations of the material structure. The effect of

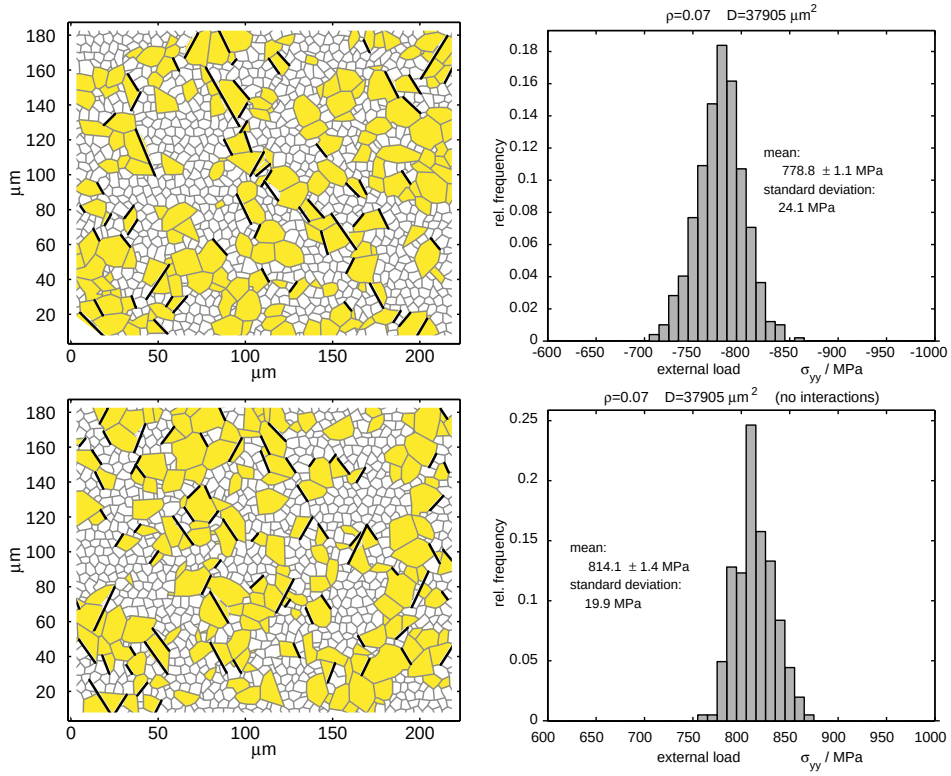

Fig. 3. Microcrack patterns forming under vertical compression increased until the crack density becomes $\rho = 0.07$. Upper: interacting cracks, lower: no interaction. (Compact two-phase material, fine and coarse grain phases with same mechanical properties.)

crack interaction is seen to be significant for rupture in contrast to the minor influence it has on overall properties of an elastic solid with random microcracks.

Structural disorder promotes the quasi-brittle mode of rupture that is preceded by distributed damage. Disorder can be introduced in the microstructure by the nature and size of grain phases, eigenstrains, and defects like pores. The presence of pores of comparable size was found to favour distributed damage. If loading is by internal pressure in the pores, however, the mode of rupture can be brittle or quasi-brittle depending on topological details of the microstructure (Fig. 4).

Fracturing under internal pore pressure modifies the concept with respect to the local criterion of fracture. Superposition of elementary solutions still gives an estimate for the stress distribution prior to the initiation of cracking and identifies critical locations. But, the particular loading condition favours that cracks emanate from pores boundaries. Such a pore/crack configuration suggests computation of the energy release rate as from the stress intensity factor instead from the stress field. Recalling the relation

$$G = \frac{K^2}{E} \tag{12}$$

between the energy release rate G, the stress intensity factor K, and the elastic modulus E, the energy release integral for the virtual separation of a grain interface in Eq. (11) is evaluated locally, with expressions for K available in the literature (Berezhnitskii, 1966). For the straight crack emanating from an elliptical pore (Fig. 5) there is

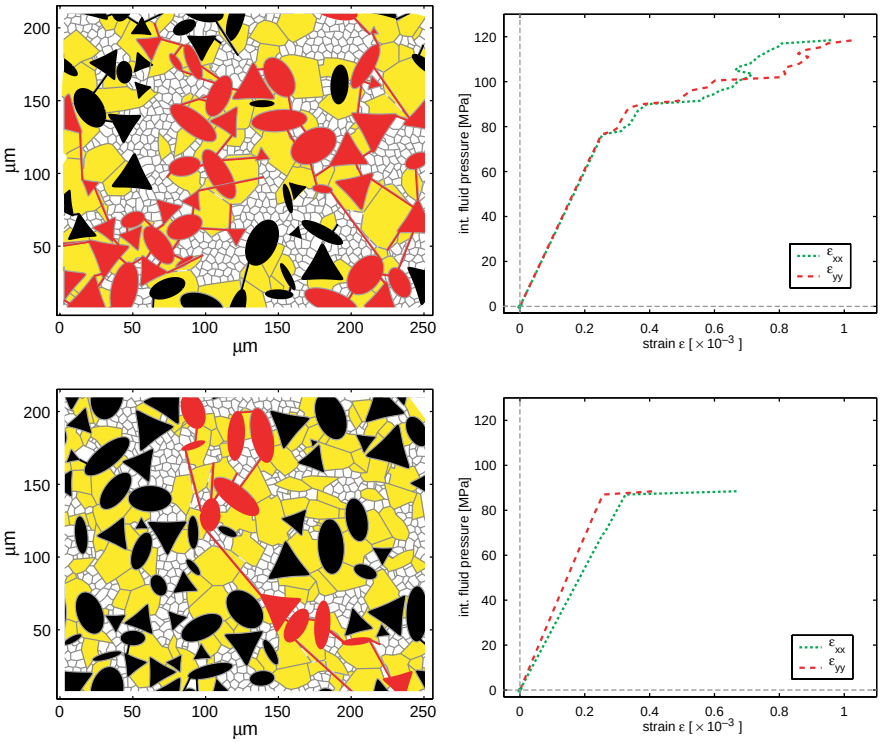

Fig. 4. Porous material subject to internal pore pressure (pores in black, fine grains in white, coarse grains in yellow; rupture patterns of pore/crack networks highlighted in red). Quasi-brittle (upper) and brittle mode of rupture (lower) under pore pressure. (For interpretation of the references in colour in this figure legend, the reader is referred to the web version of this article.)

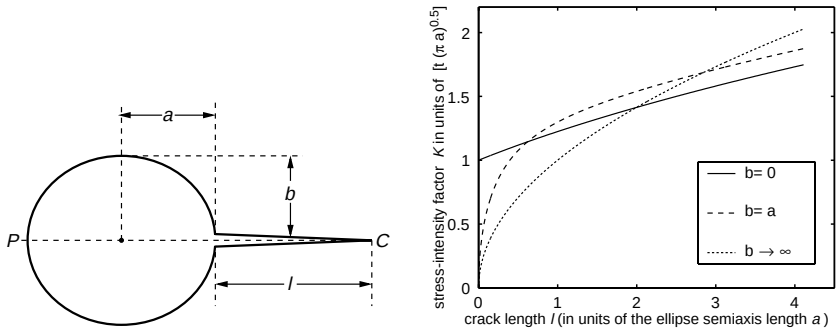

Fig. 5. Crack/pore configuration and stress intensity factor.

$$\left(\frac{K}{\pi t}\right)^2 = \left(a+\frac{l}{2}\right)\frac{(1+l/a)^2-1}{(1+l/a)^2-m}\,\frac{(1+l/a)+1}{(1+l/a)+m}, \qquad m=\frac{a-b}{a+b}, \tag{13}$$

where t denotes the intensity of biaxial tension resp. of the pressure acting in the pore. A graphical representation of the above relationship is included in the figure. Modifications necessary for more general pore/crack geometries have been performed (Doltsinis and Dattke, 2001). The local nature of stress intensity factors resulting from isolated solutions does not support consideration of interactions in the present case, but the effect is not significant here because cracking is essentially driven by the internal pressure.

4. Variability of strength

Brittleness is known to enhance the variability of strength among specimens from the same material because of fluctuations in the microstructure. The subsequent numerical experiments refer to porous material under internal pressure, for which brittle failure by separation is likely to occur. Fig. 6 demonstrates the variability of strength with the topology of circular pores, all other parameters kept constant. Positioning the pores at random within the microstructure reveals separation patterns differing among individual realizations. The computed value of the appertaining pressure varies up to 20%. These observations suggest rigorous statistical treatment based on synthetic random sampling.

Fig. 7 collects results from studies on statistical samples. Distinct realizations have been obtained by randomly positioning the pores within the grain network, all other characteristics maintained; the circular pores are of the same size. The histograms refer to the value of the percolation pressure that is when the specimen separates by a flaw chain extending from one border to the opposite. Comparison between the first and the second row indicates the effect of an increasing specimen size: the ultimate pressure is lowered as suggested by the weakest link hypothesis while the sensitivity to the topology of the pores diminishes, indicating that the specimen becomes more homogeneous. The pore size is quantified by the specific perimeter of the porous phase. At constant porosity, smaller pores displace the ultimate pressure to higher values as does also a finer grain size.

Fig. 8 demonstrates the influence of the pore shape. For equal porosity and specific perimeter of the porous phase, the microstructure with elliptical cavities sustains lower pressure than the circular. At the same time, the scatter of the strength is increased since both position and orientation of the pores are varied. An increase of porosity is found to reduce the strength, as expected.

The effect of an increasing specimen size on the strength is summarized in Figs. 9 and 10. The diagrams contrast structures that contain circular pores with varying diameter (polydisperse), and alternatively pores

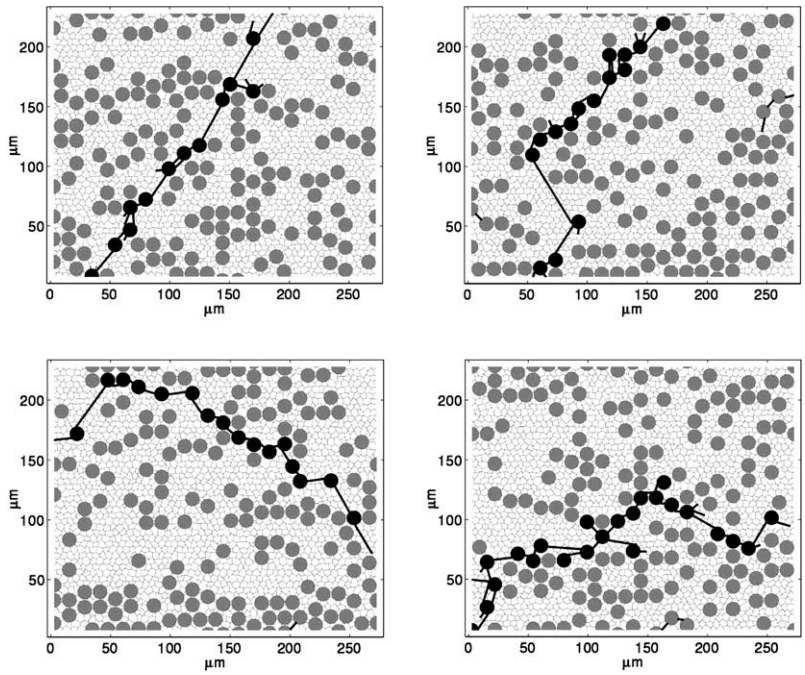

Fig. 6. Variability of fracture pattern and strength with pore topology. Specimens separate at pressure values of 171.6, 205.4, 174.2, and 187.2 MPa respectively (left to right from above).

with unique diameter (monodisperse) equal to the polydisperse mean. Following Fig. 9 the mean value of the strength diminishes for larger specimens, tending to a low but non-zero limit. The strength is lower if the pore diameter varies. In this connection we consider for the polydisperse case (index 2) the specific perimeter of the porous phase L_A,

$$L_{A2} = \frac{\pi}{A}\sum_{i=1}^{n_2} d_i = \frac{\pi}{A}(n_2\bar{d}) \tag{14}$$

and the porosity A_A,

$$A_{A2} = \frac{\pi}{4A}\sum_{i=1}^{n_2} d_i^2 = \frac{\pi}{4A}[n_2\bar{d}^2 + (n_2-1)s^2]. \tag{15}$$

In the above, A denotes the area of the specimen, n the number of the circular pores and d the diameter. Furthermore, we introduced the mean pore diameter in the specimen

$$\bar{d} = \frac{1}{n_2}\sum_{i=1}^{n_2} d_i \tag{16}$$

and its variance

$$s^2 = \frac{1}{n_2-1}\sum_{i=n}^{n_2}(d_i-\bar{d})^2 = \frac{1}{n_2-1}\left(\sum_{i=1}^{n_2} d_i^2 - n_2\bar{d}^2\right), \tag{17}$$

with s giving the standard deviation.

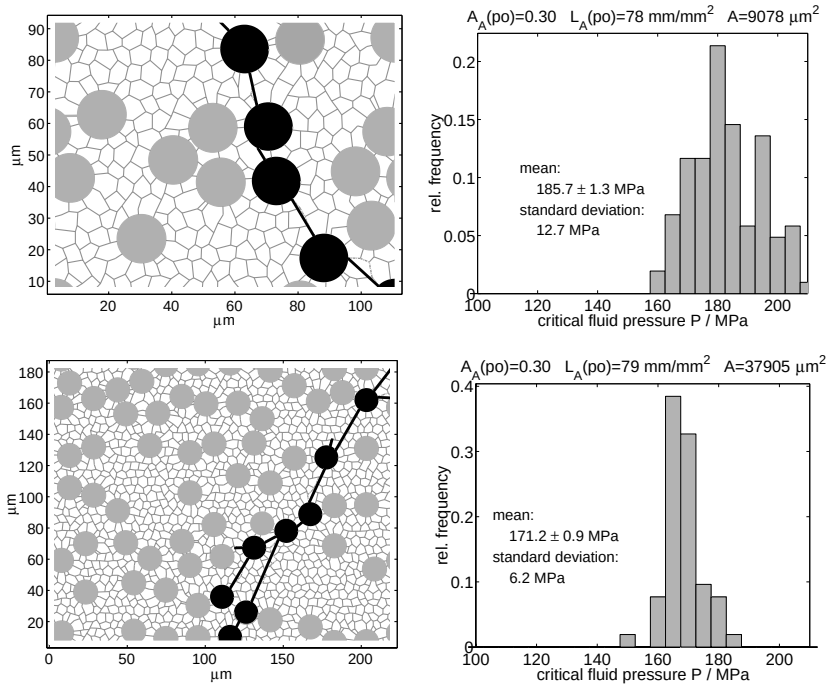

Fig. 7. Effect of specimen size on strength. Specimen area A is increased at constant porosity A_A and specific perimeter L_A of porous phase.

In the monodisperse case ($d = \text{const.} = \bar{d}, \text{index } 1$), specific perimeter and porosity read

$$L_{A1} = \frac{\pi}{A}(n_1 \bar{d}) \tag{18}$$

and

$$A_{A1} = \frac{\pi}{4A}(n_1 \bar{d}^2), \tag{19}$$

respectively. From Eqs. (14) and (18) for the specific perimeter:

$$\frac{L_{A2}}{L_{A1}} = \frac{n_2}{n_1} \tag{20}$$

and from Eqs. (15) and (19) for the porosity

$$\frac{A_{A2}}{A_{A1}} = \frac{n_2}{n_1} + \frac{n_2 - 1}{n_1}\left(\frac{s}{\bar{d}}\right)^2. \tag{21}$$

Consequently, for equal specific perimeter ($L_{A2}/L_{A1} = n_2/n_1 = 1$) the polydisperse configuration exhibits a higher porosity ($A_{A2}/A_{A1} > 1$). In the numerical experiments the porosity was maintained ($A_{A2}/A_{A1} = 1$) in which case the specific perimeter of the polydisperse porous phase is lower ($L_{A2}/L_{A1} = n_2/n_1 < 1$). But, both increasing porosity and decreasing specific perimeter have been found to diminish the strength (Doltsinis and Dattke, 2001) which is confirmed by comparing the results for monodisperse and polydisperse specimens in Fig. 9.

Fig. 10 shows the scatter of strength caused by a random variation of the topology of the pores. It is seen that for the monodisperse and the polydisperse configurations the standard deviation decreases when the

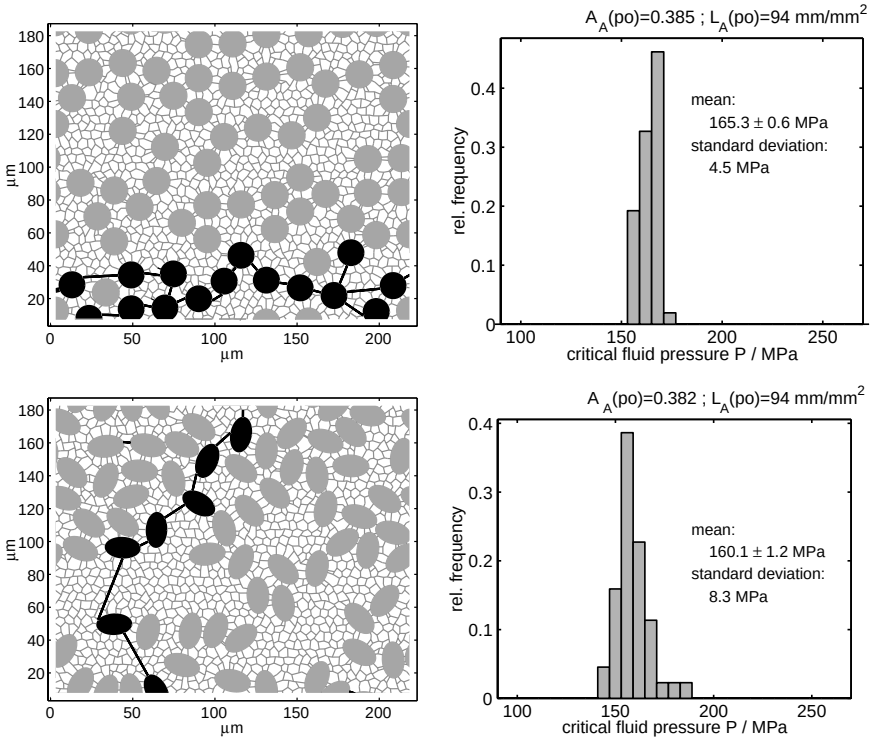

Fig. 8. Influence of pore shape on strength.

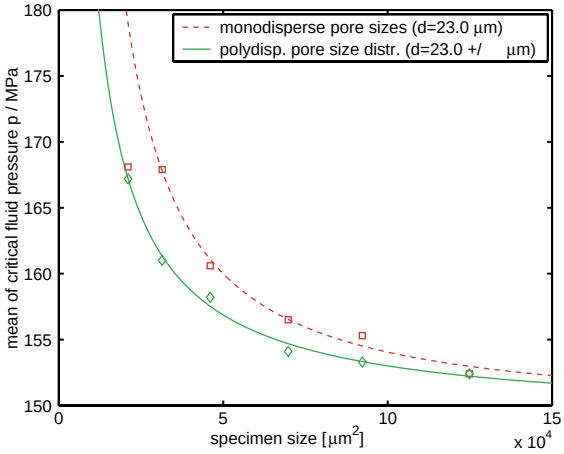

Fig. 9. Variation of mean strength with specimen size. The curves result from least square fitting of the numerical data.

specimen dimensions grow, faster and tending to zero if the pores are of equal diameter. This demonstrates the effect of an increasing homogeneity within the statistical sample.

Because of the scatter of strength in brittle rupture, probability distributions appear useful beside mean value and variance, and are often characterized by Weibull statistics (Weibull, 1951). In this connection the probability of failure P_f of the material specimen at pore pressure p is assumed given by

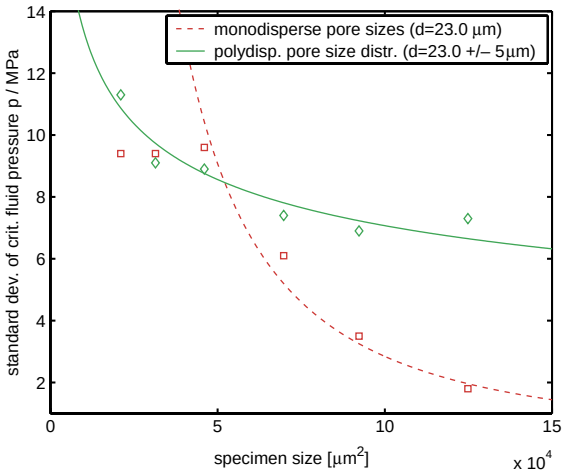

Fig. 10. Standard deviation of strength vs. specimen size.

$$P_{\mathrm{f}} = 1 - \exp\left[-\frac{V}{V_0}\varphi(p)\right], \tag{22}$$

in conjunction with the particular form

$$\varphi(p) = \left(\frac{p - p_u}{p_0}\right)^m. \tag{23}$$

The exponential in Eq. (22) helps account in a simple manner for the effect of the actual volume V with respect to volume V_0 that refers to the specifying test series. The power form for $\varphi(p)$, suggested for simplicity, usually works satisfactorily. No failure occurs for $p \leqslant p_u$; the so-called characteristic strength p_0 is associated with $P_{\mathrm{f}} = 1 - 1/\mathrm{e}$ in the test with $V = V_0$.

Projection of the numerical experiments on the Weibull probability distribution of the strength values is depicted in Figs. 11–14. Fig. 11 refers to test series at different specimen sizes. In this logarithmic diagram the Weibull function given by Eqs. (22) and (23) would appear as a straight line with slope m that crosses the strength axis at $p - p_u = p_0$ (see Fig. 12). Usually, p_u is taken zero. The results can hardly support the constancy of the parameter m in a series. Although the situation improves for larger specimens with a polydisperse porous phase (Fig. 12), a multimodal approximation (Weibull, 1951) seems more appropriate. The branch associated with higher strength values might lead one to suppose here the quasi-brittle mode of fracture, but the results in Fig. 6 advise caution. Fitting the Weibull function nevertheless with the numerical results of Fig. 11 supplies the diagrams in Figs. 13 and 14.

Fig. 13 shows the characteristic strength p_0 to decrease as specimens are taken larger, which expresses the weakening effect of increasing specimen dimensions already observed in Fig. 11. Fig. 14 demonstrates the variation of the exponent m. For circular pores of unique diameter (monodisperse) the augmentation of the m-value with specimen size reflects the diminution of scatter as a result of statistical homogeneity. In contrast, the exponent m is seen to approach a constant value if the pore diameter varies in the specimen (polydisperse), which rather suits actual microstructures. The above is but another interpretation of the observations in Fig. 10. It signifies that with the equally sized pores the specimen dimensions may be increased up to a deterministic representation of the rupture strength; for the variable pores a certain least specimen size is required in order that the statistical description of the rupture strength becomes stationary.

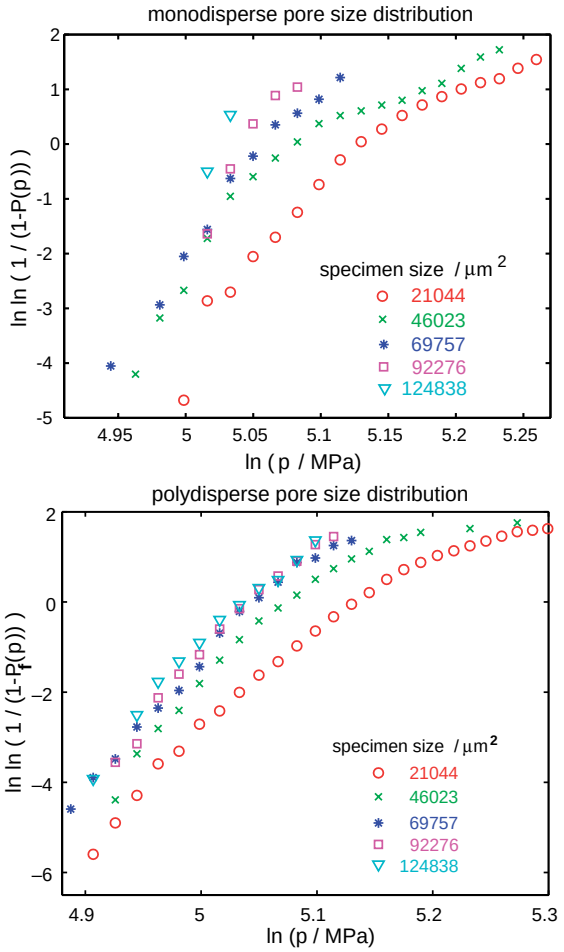

Fig. 11. Probability of rupture strength in Weibull plot. Monodisperse porous phase (upper). Polydisperse porous phase (lower).

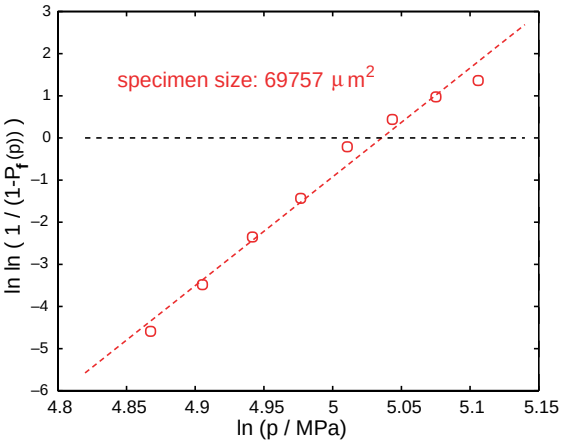

Fig. 12. Strength of larger specimen tends to reproduce Weibull distribution (polydisperse porous phase).

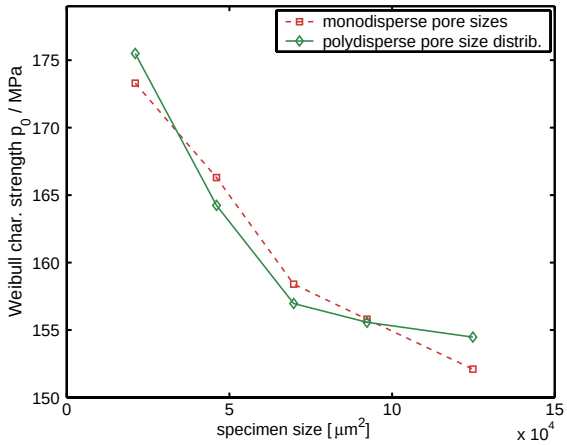

Fig. 13. Variation of characteristic strength p_0 with specimen size.

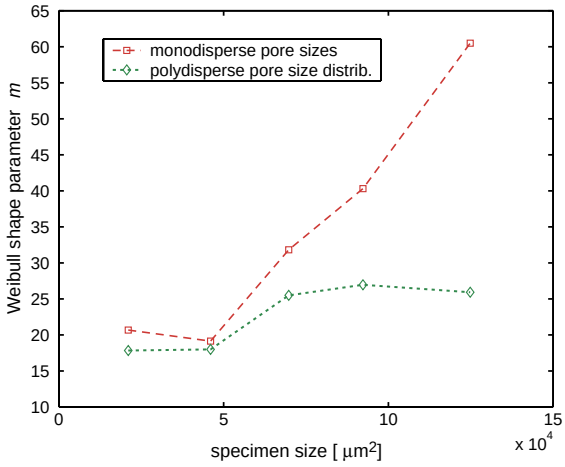

Fig. 14. Variation of exponent m with specimen size.

A remark is due in connection with the parameter p_u, the lowest ultimate strength, usually neglected. As has already been outlined, with increasing specimen dimensions the value of separation strength tends to become stationary, low but non-zero. This is because the variation of pore size is limited to within a finite interval. As a consequence the lowest ultimate strength p_u cannot be expected to be zero in this case and gains importance.

5. Concluding remarks

An analysis of rupture of brittle materials has been performed by numerical modelling on the microscale along with statistical considerations. The computer algorithm for brittle rupture accounts for the material microstructure, which is subject to synthetic random sampling at constant macroscopic data.

The studies on the microscale help enlarging knowledge on elementary physical processes; statistics explores the sensitivity of collective behaviour to the variability of the material structure. Reproduction of

actual values is not intended in this study. For this reason details on input data have been omitted here, but are stated elsewhere (Dattke, 2003). The numerical model interprets the role of participating parameters such as structural characteristics, loading, and specimen size. The two-dimensional approach employed investigates essential effects at reasonable effort in theory and computation. As a result of the reduced dimensionality of the model the predictions may be considered to be rather conservative estimates of three-dimensional situations.

Changing the scale of observation and employing statistics provides an insight into the role of distinct microstructural parameters, but is no substitute for thinking about the problem of characterizing the macroscopic properties of the material.

References

Berezhnitskii, L.T., 1966. Propagation of cracks terminating at the edge of a curvilinear hole in a plate. Sov. Mater. Sci. 2, 16–23.

Dattke, R., 2003. Modelling the microstructure and simulation of progressive fracturing in brittle porous ceramics. Doctoral Dissertation, Faculty of Aerospace Engineering, University of Stuttgart.

Doltsinis, I., 1998. Issues in modelling distributed fracturing in brittle solids with microstructure. In: Idelsohn, S.R., et al. (Eds.), Computational Mechanics—New Trends and Applications, (CD-ROM) CIMNE, Barcelona.

Doltsinis, I., Dattke, R., 2001. Modelling the damage of porous ceramics under internal pressure. Comput. Methods Appl. Mech. Eng. 191, 29–46.

Hrennikoff, A., 1941. Solution of problems of elasticity by the framework method. J. Appl. Mech. 63, A169–A175.

Kachanov, M., 1987. Elastic solids with many cracks: a simple method of analysis. Int. J. Solid Struct. 23/1, 23–43.

Kachanov, M., Tsukrov, I., Shafiro, B., 1994. Effective moduli of solids with cavities of various shapes. Appl. Mech. Rev. 47, 151–174.

Krajcinovic, D., 1996. Damage Mechanics. Elsevier, North-Holland, Amsterdam.

Louis, E., Guinea, F., Flores, F., 1986. The fractal nature of fracture. In: Pietronero, L. (Ed.), Fractals in Physics. Elsevier, North-Holland, Amsterdam.

Srolovitz, D.J., Beale, P.D., 1988. Computer simulation of failure in an elastic model with randomly distributed defects. J. Am. Ceram. Soc. 71, 362–369.

Treiniés, K.A., 1988. Numerisches Stabwerksmodell zur Simulation des Verhaltens eines keramischen Werkstoffes bei Schaedigung durch Mikrorisse. Diploma Thesis, ICA, University of Stuttgart.

Tsukrov, I., Kachanov, M., 1997. Stress concentrations and microfracturing patterns in a brittle-elastic solid with interacting pores of diverse shapes. Int. J. Solid. Struct. 34, 2887–2904.

Weibull, W., 1951. A statistical distribution function of wide applicability. ASME J. Appl. Mech., 293–297.